



Statistical models to provide meaningful information to GNSS users in the presence of ionospheric scintillation

S. Vadakke Veetil¹  · M. Aquino¹ 

Received: 3 June 2020 / Accepted: 29 December 2020
© The Author(s) 2021

Abstract

Ionospheric scintillation is one of the most challenging problems in Global Navigation Satellite Systems (GNSS) positioning and navigation. Scintillation occurrence can not only lead to an increase in the probability of losing the GNSS signal lock but also reduce the precision of the pseudorange and carrier phase measurements, thus leading to positioning accuracy degradation. Statistical models developed to estimate the probability of loss of lock and Geometric Dilution of Precision normalized 3D positioning errors as a function of scintillation levels are presented. The models were developed following the statistical approach of nonlinear regression on data recorded by Ionospheric Scintillation Monitoring Receivers operational at high and low latitudes. The validation of the probability of loss of lock models indicated average correlation coefficient values above 0.7 and average Root Mean Squared Error (RMSE) values below 0.35. The validation of the positioning error models indicated average RMSE values below 10 cm. The good performance of the developed models indicates that these can provide GNSS users with information on the satellite loss of lock probability and the error in the 3D position under scintillation.

Keywords Global navigation satellite systems · Statistical models · Ionospheric scintillation · Positioning errors · Probability of loss of lock

Introduction

The earth's ionosphere is the single largest contributor to the Global Navigation Satellite System (GNSS) positioning error budget. In particular, a phenomenon known as Ionospheric scintillation, characterized by fluctuations in the GNSS signal amplitude and phase, may seriously disrupt satellite tracking and degrade system accuracy, reliability and integrity (Kintner et al. 2001). The day-to-day variability in scintillation occurrence and its dependence on local time, season, latitude, longitude, solar and geomagnetic activity are well known and discussed in Basu et al. (2002) and Kintner et al. (2007). The two global regions where scintillation occurs predominantly are the equatorial to low latitude regions, extending from about 20°N to 20°S geomagnetic latitudes, and the high latitude regions, extending from 65° to 90° geomagnetic latitudes. However, in these two regions, the processes governing the generation of

scintillation causing plasma density irregularities are quite different, thereby leading to significant differences in the observed characteristics of the scintillation effects (Jiao and Morton 2015).

Ionospheric scintillation can significantly impact the GNSS receiver signal tracking performance. Rapid amplitude fluctuations associated with scintillation can cause the signal-to-noise ratio to drop below the receiver threshold, and when this depth of fading exceeds the fade margin of the receiver, signal loss and cycle slips occur (Akala et al. 2012). A measure of the amplitude scintillation is provided by the S4 index, defined as the standard deviation of the received signal power normalized to the average signal power. The rapid phase fluctuations associated with scintillation may cause the frequency Doppler shift in the signal carrier to exceed the receiver's Phase Locked Loop (PLL) bandwidth, and loss of phase lock may be observed (Humphreys et al. 2005). Phase scintillation is characterized by the SigmaPhi (σ_ϕ) index, defined as the standard deviation of the detrended carrier phase computed over intervals of 1, 3, 10, 30 and 60 s, based on 50 Hz measurements. Scintillation can increase the tracking jitter variance measured at the output of the PLL and the correlation

✉ S. Vadakke Veetil
v.sreeja@gmail.com

¹ Nottingham Geospatial Institute, University of Nottingham,
Triumph Road NG7 2TU, Nottingham, UK

between scintillation levels and phase tracking jitter at low and high latitudes can be represented by a quadratic fit as shown, respectively, in Sreeja et al. (2012) and Aquino and Sreeja (2013). Statistical models developed to estimate the standard deviation of the receiver PLL tracking jitter as a function of scintillation levels are presented in Vadakke Veetil et al. (2018a). Skone et al. (2001) reported that during strong scintillation the availability of carrier phase observations is limited due to loss of signal lock, with significant impact on positioning applications. Using data from equatorial and auroral regions, Doherty et al. (2003) demonstrated that scintillation can have an adverse effect on receiver performance, resulting in increased cycle slips and losses of lock. Additionally, even if receivers are able to maintain lock during moderate to strong scintillation conditions, the errors due to scintillation propagate to the GNSS measurements, leading to a degradation in positioning accuracy (Pi et al. 2017). Statistical models to estimate the 3D positioning errors as a function of scintillation levels are presented in Veetil et al. (2018b), which demonstrated that if nowcasted scintillation information is available, then the developed statistical models can be used to estimate the nowcasted 3D positioning errors on a global scale.

With the increasing reliance on GNSS for several modern life applications such as connected & autonomous vehicles, infrastructure monitoring, offshore operations, precision agriculture and mapping, precise ionospheric information can contribute to the understanding of the impact of significant ionospheric related events on our technology based society. In this context, the “Ionosphere Prediction Service” (IPS), a project funded by the European Commission (EC) under Horizon 2020, in the frame of the Galileo program, aimed to translate the information on the state of the ionosphere into GNSS user-devoted products through the design and development of an ionospheric prediction service prototype. Further details about the IPS project are available in Vadakke Veetil et al. (2019) and from the project web portal (<https://ips.gsc-europa.eu>).

Statistical models have been developed in the context of the IPS project to estimate the probability of loss of lock and Geometric Dilution of Precision (GDOP) normalized 3D positioning errors at high and low latitudes as a function of the scintillation levels. The development of these models for the first time based on long-term data representing scintillation levels actually observed in the different global regions is presented. The considerable size of the data set and the scintillation levels that it covers provide a large and representative enough sample to ensure the statistical robustness of the models, which are validated in the research. The next section describes the data and methodology adopted in the development of the models, followed by a section presenting the results and discussions. Finally, the conclusions are presented.

Data and methodology

The data collected by Ionospheric Scintillation Monitoring Receivers (ISMRs) in operation at the high and low latitudes during the years of 2012–2015 have been exploited to develop the statistical models to estimate the probability of loss of lock on the Global Positioning System (GPS) L1 frequency and the GDOP normalized 3D positioning errors. Following a statistical approach of nonlinear regression (Seber and Wild 2003), models have been developed incorporating the dependence on scintillation levels, as represented by the scintillation indices and the root mean square of the Rate of change of slant Total Electron Content (STEC) index (ROT_{rms}). The ROT_{rms} is a commonly used measure of ionospheric activity characterizing rapid variations of TEC and is strongly related to scintillation (Pi et al. 1997; Basu et al. 1999). Two types of ISMRs, namely the Novatel GSV4004B and the Septentrio PolaRxS, and two types of geodetic receivers, namely Topcon NET-G3A and Trimble NETR9 have been used in this study. Table 1 shows the geographic latitude and longitude of the stations along with the geomagnetic latitude and the GNSS receiver type.

Table 1 Geographic latitude and longitude of the stations used in the statistical model development and validation along with the geomagnetic latitude and GNSS receiver type

ID	Station	Lat (°N)	Long (°E)	Geomagnetic Lat (°N)	Receiver Type
NYA	Ny-Ålesund	78.92	11.93	75.98	GSV4004A (2005–2007) GSV4004B (2008–2015)
IQL	Iqaluit	63.76	-68.51	73.26	Topcon NET-G3A
IQA	Iqaluit	63.74	-68.54	73.24	GSV4004B
BRO	Brønnøysund	65.46	12.22	64.42	PolaRxS
PAL	Palmas	-10.12	-48.18	-1.22	PolaRxS
PRU	Presidente Prudente	-22.07	-51.24	-12.88	PolaRxS
UFP	Curitiba	-25.45	-49.23	-16.26	Trimble NETR9
POA	Porto Alegre	-30.04	-51.07	-20.81	PolaRxS

The number of days during the years of 2012–2015 used in the development of the probability of loss of lock and positioning error models at high and low latitudes is shown in Table 2. The geographic location of the stations is shown in Fig. 1.

The two types of ISMR taking part in this study use similar algorithms to provide the scintillation indices, namely S4 and σ_ϕ (Sreeja et al. 2011). The one-minute S4 and σ_ϕ indices recorded on the GPS L1 frequency per satellite-receiver link are used in this study. Both types of ISMR also record the uncalibrated STEC and the differential TEC (dTEC) values at every 15 s per satellite-receiver link (Van Dierendonck et al. 1993; Septentrio PolaRxS application manual 2010). The uncalibrated STEC is referred to as the STEC value estimated without taking into account receiver and satellite differential code biases. The dTEC values refer to the change in TEC over the four 15 s intervals during the last minute estimated using the phase observations of the GPS legacy signals L1C/A and L2P. The ROT_{rms} per satellite-receiver link used in this study is computed by calculating the root mean square (rms) of the four dTEC values provided by the ISMR over each minute so that it matches the time resolution of the scintillation indices. It is to be noted that inconsistencies exist when ROT_{rms} is estimated from multiple GNSS receiver types or different signal combinations of a single receiver (Yang and Liu 2017). The development of the models based on ROT_{rms} is intended to support the estimation of the probability of loss of lock and positioning errors over regions where the scintillation indices or the ISMR data are

Table 2 Number of days during the years 2012 to 2015 used in model development

Station	2012	2013	2014	2015
IQA (high latitude)	297	297	289	168
PRU (low latitude)	314	301	322	300

unavailable. This is because the ROT_{rms} can be computed from uncalibrated STEC values that can be estimated using data from any dual-frequency GNSS receiver. The differencing of the STEC values over time to estimate the ROT will remove any biases in the STEC measurements. The scintillation levels, as characterized by the scintillation indices and ROT_{rms}, have been estimated only for satellites with elevation angle greater than 20° in order to remove the contribution from non-scintillation related errors such as multipath. The ranges of scintillation indices and ROT_{rms} values used in the model development are 0–1 and 0–5, respectively.

Figures 2 and 3 show the temporal variations in the ROT_{rms} (top), σ_ϕ (middle) and S4 (bottom) recorded by the 6 ISMRs used in this study on strong scintillation days, respectively, at the high and low latitudes. A good correlation between the scintillation indices and ROT_{rms} can be observed from Figs. 2 and 3. During the scintillation periods, the ROT_{rms} increases to values greater than 1 TECU/min. The enhancements in ROT_{rms} closely follow those of

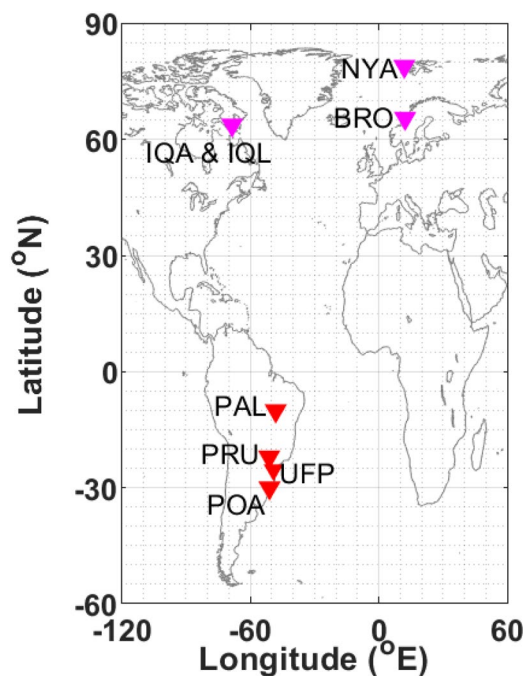


Fig. 1 Geographical location of the stations listed in Table 1

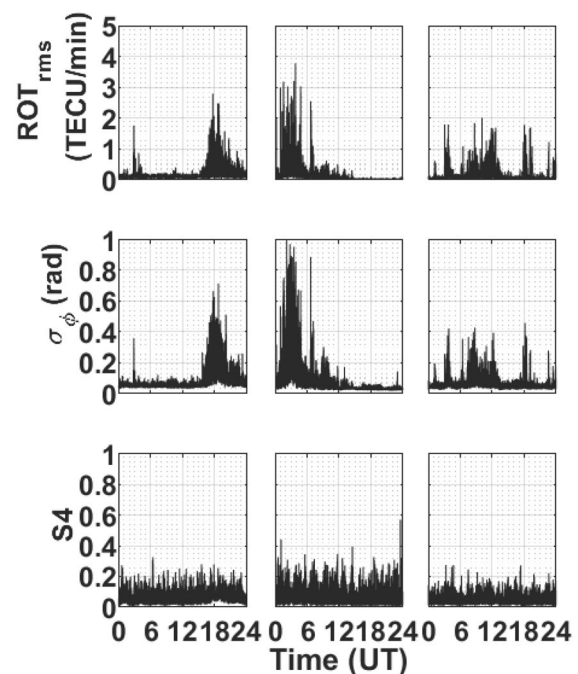


Fig. 2 Temporal variations of ROT_{rms} (top), σ_ϕ (middle) and S4 (bottom) recorded at the high latitude stations IQA (left) on December 14, 2015, BRO (middle) on November 14, 2012 and NYA (right) on March 9, 2008

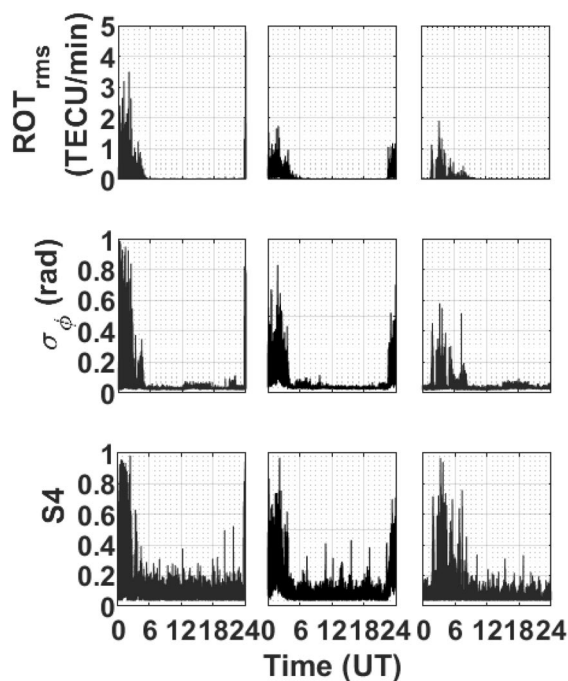


Fig. 3 Temporal variations of ROT_{rms} (top), σ_{ϕ} (middle) and S4 (bottom) recorded at the low latitude stations PRU (left) on February 14, 2014, PAL (middle) on October 24, 2013 and POA (right) on January 2, 2014

the scintillation indices, confirming that ROT_{rms} could be used to represent the presence of ionospheric irregularities leading to the occurrence of scintillation. It can be observed from Figs. 2 and 3 that the ROT_{rms} is a good indicator of phase scintillation at high latitudes, and of both amplitude and phase scintillation at low latitudes, a feature in agreement with that presented in Pi et al. (2013). These observed differences in correlation can be partially attributed to the physical processes causing plasma density irregularities leading to the generation of scintillation in the different latitude regions (Jiao and Morton 2015).

The loss of lock events defined in this study was identified for each satellite-receiver link from the L1 lock time output by the ISMRs at every one-minute, indicating for how long the receiver has been successfully tracking the carrier phase on the L1 signal. A loss of lock was considered detected when the lock time was less than 60 s for visible satellites with elevation angle greater than 20° . In the development of the probability of loss of lock models, the entire dataset at each high and low latitude station was classified considering two subsets: (1) samples for which a loss of lock occurred within the 1 min window and (2) samples which are more than 4 min away from the next loss of lock event. The second subset is defined to account for the 4 min required by the receiver to settle after a loss of lock event (Van Dierendonck et al. 1993). These subsets

were binned according to the scintillation levels, with a step size of 0.05 and 0.25 for the scintillation indices and ROT_{rms} , respectively. The probability of loss of lock in each bin was computed as:

$$Pr ob\ lol = N_{lol} (> 8)/N \quad (1)$$

where N_{lol} is the number of samples in subset 1, and N is the total number of samples considering both subsets 1 and 2. In order to remove the contribution of bins with poor statistics, the probability for a bin was not calculated if the total number of samples was fewer than 8 in that bin. The distribution of the scintillation level values covered by the four year long data (2012–2015) used in the model development is shown in Table 2 in Vadakke Veetil et al. (2018a). It is clear that the number of samples decreases with the increase in the scintillation levels and is 5 when ROT_{rms} is in the range of 4.5–5. This is the reason for applying a threshold of 8 samples to calculate the probability.

The GDOP normalized 3D positioning error models have been developed based on Precise Point Positioning (PPP) solutions using GPS data provided by the ‘GPSPACE’ software available from NRCan (National Resources Canada) as an online tool (Donahue et al. 2015). PPP is a GNSS carrier phase based high accuracy positioning technique utilizing undifferenced dual-frequency code and phase observations (Malys and Jensen 1990; Zumberge et al. 1997; Kouba and Héroux 2001). The GPSPACE applies the ionospheric free linear combination from dual-frequency data, thus eliminating the first order ionospheric error. The GPS data were processed in kinematic mode considering a satellite elevation mask of 10° , a priori standard deviations of 2 m and 0.015 m, respectively, for pseudorange and carrier phase observations, final precise orbits and clocks from the International GNSS Service (IGS) and the tropospheric zenith delay estimated as a random walk process (5 mm/h). The 3D positioning error at every minute after PPP convergence was computed as the difference of the estimated coordinates from the known station coordinates used as ground truth. The accuracy of a PPP solution is also influenced by the satellite-receiver geometry measured by the DOP parameter. The DOP at each epoch is related to the observational geometric configuration between the satellites and the receiver, such that the positioning accuracy may be significantly degraded when a small number of satellites is available. To remove the effects of the satellite-receiver geometry on the positioning solution, the calculated 3D positioning errors were normalized by the GDOP to develop the statistical models. The scintillation levels as represented by the scintillation indices and ROT_{rms} were averaged over each one-minute interval to match the time resolution of the GDOP normalized 3D positioning errors.

The user at a particular location and time needs to multiply the model output by the instantaneous GDOP at that location and time to calculate the absolute 3D positioning error.

The validation of the developed statistical models was carried out by adopting a data sacrifice strategy whereby selected data covering scintillation and non-scintillation days during different seasons has been left out during the development phase of the models. The criteria for categorizing days as scintillation or non-scintillation for the high and low latitudes was based on the temporal variations of σ_ϕ and S4, respectively. The following criteria was applied to categorize the day as scintillation: (1) as this study focuses on moderate to strong levels of scintillation, the threshold for S4 and σ_ϕ was set as 0.3; (2) the satellite elevation cut off was set as 20°; (3) the S4 or σ_ϕ values remain above the threshold for more than 15 min; (4) for equatorial and low latitude stations, this 15-min interval refers to the post sunset period and for high latitudes, this 15-min interval refers to

any time during the day. Days on which the S4 or σ_ϕ values were less than 0.3 for the whole day were categorized as non-scintillation. In addition, to confirm the selection of scintillation and non-scintillation days manual visual inspection of the figures illustrating the temporal profiles of the S4 and σ_ϕ was performed. The list of days used for the validation of the developed models at stations IQA, BRO, NYA, PRU, PAL and POA are shown in Table 3. It is to be noted that the days listed for IQA and PRU were chosen to validate the models at stations IQL and UFP equipped with Topcon NET-G3A and Trimble NETR9 receivers, respectively.

The goodness of fit of the probability of loss of lock models was evaluated by using the correlation coefficient, R and Root Mean Squared Error (RMSE) of the residuals. R is a measure of how well the model estimates the variability in the observations and a higher value for R indicates that the model represents the trend of the observations well. The RMSE is a measure of how accurately the model estimates the observations themselves and a low value of the RMSE

Table 3 Scintillation and non-scintillation days selected for validation

Station	Year	Scintillation (m/d)	Non-scintillation (m/d)
IQA, IQL	2012	1/22; 2/6; 3/3; 5/23; 6/5; 7/15; 8/16; 9/30; 10/8; 11/14; 12/26	1/5; 2/17; 3/30; 5/17; 6/9; 7/13; 8/10; 9/29; 10/20; 11/9; 12/7
	2013	1/17; 2/14; 3/17; 4/24; 5/25; 6/1; 8/16; 9/22; 10/30; 11/7; 12/14	1/5; 2/6; 3/22; 5/15; 6/12; 7/2; 8/8; 9/27; 10/5; 11/27; 12/22
	2014	1/1; 3/13; 4/7; 5/22; 6/19; 7/30; 8/27; 9/19; 10/10; 11/10	1/31; 2/13; 4/22; 5/14; 6/27; 7/23; 8/23; 10/17
	2015	5/26; 6/25; 7/25; 8/15; 10/15; 11/7; 12/14	5/23; 6/4; 7/2; 8/14; 10/26; 11/12; 12/30
BRO	2011	9/10; 10/25; 11/29	9/5; 10/18; 11/15
	2012	1/23; 3/9; 5/23; 6/12; 7/16; 9/30; 10/9; 11/14	1/4; 5/4; 6/1; 7/5; 8/10; 9/13; 10/19; 11/8
	2013	3/1; 3/21; 3/30; 4/24; 5/18; 6/1; 7/15	1/7; 2/11; 3/22; 4/15; 5/3; 6/5; 7/21
NYA	2005	1/22; 2/16; 4/12; 5/15; 7/10; 8/24; 12/1	1/26; 2/22; 3/4; 5/6; 6/10; 7/24; 11/16
	2006	2/6; 3/11; 3/19; 4/10; 5/13; 9/24; 12/12	1/3; 2/25; 3/23; 4/3; 5/25; 9/16; 11/20
	2007	1/17; 2/14; 5/22; 7/14; 10/4; 12/21	1/23; 2/21; 4/16; 6/6; 8/20; 9/13
	2008	1/25; 2/10; 3/9; 12/6	1/12; 2/7; 4/14; 10/25
	2009	1/13; 2/14	1/12; 2/2
	2010	5/3; 6/16; 8/4; 10/22; 12/25	4/25; 6/23; 7/13; 10/4; 12/18
	2011	2/5; 5/28; 8/6; 12/29	1/28; 4/17; 6/29; 12/27
	2012	1/22; 2/1; 10/1; 10/18; 11/24	4/30; 7/13; 7/27; 10/15; 11/22
	2013	10/29; 11/1	9/29; 12/2
	2014	1/1; 2/12; 3/18; 5/1; 10/5; 11/7; 12/23	1/19; 4/10; 5/2; 6/12; 7/6; 8/16; 9/15
2015	1/4; 2/8; 4/2; 9/4; 10/15; 11/7	3/9; 4/8; 5/9; 6/5; 7/10; 11/24	
PRU, UFP	2012	1/5; 1/20; 2/3; 3/1; 3/5; 4/2; 9/23; 10/5; 11/5; 11/25; 12/10; 12/15	1/4; 1/19; 2/21; 3/8; 3/12; 4/3; 5/17; 6/22; 7/10; 8/31; 10/8; 11/1
	2013	1/9; 1/15; 2/3; 2/20; 3/10; 4/2; 9/26; 10/7; 10/14; 10/26; 11/8; 12/11	1/27; 2/15; 2/19; 3/22; 4/7; 5/25; 6/7; 7/5; 7/26; 8/5; 9/4; 10/15
	2014	1/7; 1/30; 2/6; 2/14; 3/8; 3/18; 9/19; 9/29; 10/4; 10/16; 11/14; 12/10	4/3; 4/15; 5/2; 5/15; 6/3; 6/26; 7/12; 7/20; 8/1; 8/15; 9/9; 9/15
	2015	1/1; 1/24; 2/5; 2/25; 3/4; 3/10; 9/26; 9/30; 10/11; 10/26; 11/23; 12/5	3/6; 3/24; 4/12; 4/22; 5/29; 6/2; 7/5; 7/23; 8/4; 9/12; 11/9; 12/21
	2013	9/12; 10/5; 10/17; 10/24; 11/8; 12/11	5/25; 6/12; 7/12; 8/5; 9/5; 10/15
PAL	2014	1/7; 1/23; 2/6; 2/18; 3/2; 3/16	4/3; 4/10; 4/11; 4/14; 4/24; 4/30
POA	2013	10/1; 10/20; 11/10; 11/27; 12/4; 12/12	5/25; 6/5; 7/12; 8/6; 9/5; 10/18
	2014	1/2; 1/23; 1/30; 2/1; 2/16; 3/13	1/13; 2/9; 2/28; 3/6; 4/1; 4/29

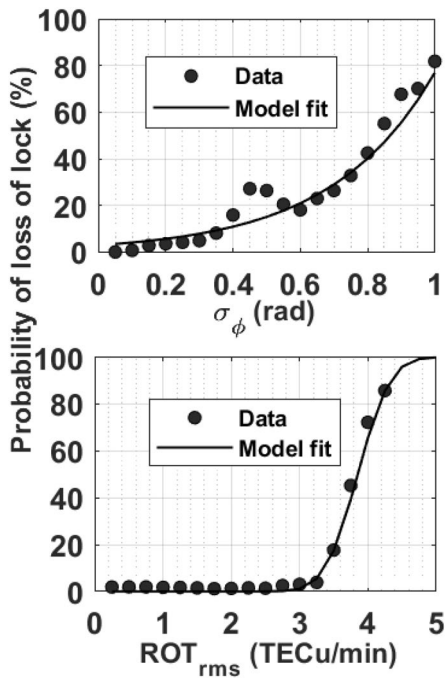


Fig. 4 Probability of loss of lock as a function, respectively, of σ_ϕ (top) and ROT_{rms} (bottom), at the station IQA

indicates the closeness between the observations and their model estimations. The goodness of fit of the GDOP normalized 3D positioning error models was evaluated by using the RMSE of the residuals.

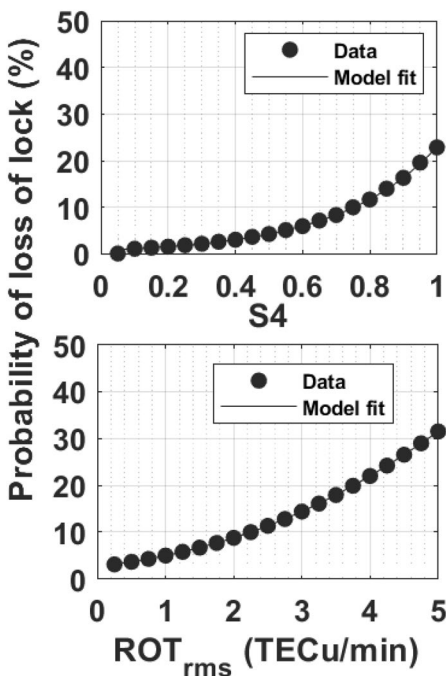


Fig. 5 Probability of loss of lock as a function, respectively, of S4 (top) and ROT_{rms} (bottom), at the station PRU

Results and discussions

The development and validation of the statistical models following the approach of nonlinear regression to estimate the probability of loss of lock at high and low latitudes are described in the following sub-section. A subsequent sub-section describes the development and validation of the GDOP normalized 3D positioning error models.

Probability of loss of lock

The statistical models for high latitude were developed using the data recorded at the IQA station in the Canadian High Arctic Ionospheric Network (Jayachandran et al. 2009), incorporating the dependence on the scintillation levels. This station was chosen because it lies at the boundary of the auroral oval, where the occurrence of high latitude scintillation is frequent (Spogli et al. 2009). Using the statistical approach of nonlinear regression, the models developed for the high latitude have the following forms:

$$Prob\ lol_{scint}^{highlat} (\%) = [0.02955 \cdot \exp(3.26 \cdot \sigma_\phi)] \cdot 100 \quad (2)$$

$$Prob\ lol_{ROT}^{highlat} (\%) = 50 \cdot [1 + \operatorname{erf}((ROT_{rms} - 3.852)/0.5287)] \quad (3)$$

where σ_ϕ is the phase scintillation index, ROT_{rms} is the rate of change of TEC index and erf is the standard error function. The top and bottom panels of Figure 4 show respectively the probability of loss of lock modeled as a function of σ_ϕ and ROT_{rms} . In this figure, the symbols indicate the observed values of probability, whereas the curve indicates the model estimated values. It can be observed from Fig. 4 that, as expected, when scintillation levels are low, very few loss of lock events are observed, and as the scintillation level increases, most samples are associated with a loss of lock. The values of σ_ϕ and ROT_{rms} corresponding to 50% probability of losing lock are 0.86 radians and 3.9 TECU/min, respectively. The results from the days listed in Table 3 for the validation of the models represented in (2) and (3) are summarized in Table 4. The table shows the average correlation coefficient R and RMSE along with the number of days used for validation.

To further assess the suitability of the models represented in (2) and (3), these models were also tested at the European high latitude stations of BRO and NYA, which did not contribute any data to the model development. The results from the validation days listed in Table 3 are shown in Table 5.

The data recorded at station PRU in Brazil was used to develop the statistical models for the low latitudes. This station was chosen because it lies close to the crest of the Equatorial Ionization Anomaly (EIA), where the occurrence

of low latitude amplitude scintillation is strong and frequent (Basu et al. 2002). The models developed for the low latitudes have the following forms:

$$Prob\ lol_{scint}^{lowlat}(\%) = [0.00797 \cdot \exp(3.36.S4)].100 \quad (4)$$

$$Prob\ lol_{ROT}^{lowlat}(\%) = 50 \cdot [1 + \operatorname{erf}((ROT_{rms} - 6.658)/4.869)] \quad (5)$$

where S4 is the amplitude scintillation index, ROT_{rms} is the rate of change of TEC index, and erf is the standard error function. The top and bottom panels of Fig. 5 show, respectively, the probability of loss of lock modeled as a function of S4 and ROT_{rms} . In this figure, the symbols and curve indicate, respectively, the observed and model estimated values of probability.

It can be noted from Fig. 5 that the probability of losing lock is 23% for S4 and ROT_{rms} values of 1 and 4, respectively. The results presented in Carrano and Groves (2010) showed that at the low latitude station of Ascension Island, an S4 value of 0.97 corresponds to 90% probability of losing lock for an Ashtech Z-XII receiver. This discrepancy in the S4 values may be attributed to the differences in tracking parameters and characteristics of the specific receivers considered in the two studies. The validation results of the models represented in (4) and (5) for the station PRU on the days listed in Table 3 are summarized in Table 6.

Similarly, to the high latitude models, the suitability of the models represented in (4) and (5) was also tested at the Brazilian low latitude stations POA and PAL, which did not contribute any data to the model development. Table 7 summarizes the validation results for these two stations for the days listed in Table 3.

The validation results presented in Tables 4, 5, 6 and 7 indicate that both the developed high and low latitude models perform well under scintillation and non-scintillation conditions. The average values of the correlation coefficient, R are mostly above 0.7, indicating a good correlation between the observed trend and the model estimated trend. The average RMSE values are below 0.35, indicating closeness between the observed and the model estimated values. These results indicate a good performance of the developed models.

The following sub-section describes the development and validation of the 3D positioning error models at high and low latitudes as a function of the scintillation levels.

GDOP normalized 3D positioning error

Similarly to the probability of loss of lock models, the statistical models to estimate the 3D positioning errors at high and low latitudes were developed following the approach of nonlinear regression using data recorded at the IQA and PRU stations, respectively. The models developed for the high and low latitudes have the forms represented, respectively, in equations (6), (7) and (8), (9) and shown in Veettil et al. (2018b):

$$3D\ poserr_{norm\ scint}^{highlat}(m) = [0.0076 \cdot \exp(7.6639 \cdot \sigma_\varphi)] \quad (6)$$

$$3D\ poserr_{norm\ ROT}^{highlat}(m) = [0.0178 \cdot \exp(1.5110 \cdot ROT_{rms})] \quad (7)$$

$$3D\ poserr_{norm\ scint}^{lowlat}(m) = [0.0241 \cdot \exp(6.2991 \cdot S4_{rms})] \quad (8)$$

$$3D\ poserr_{norm\ ROT}^{lowlat}(m) = [0.0233 \cdot \exp(0.5765 \cdot ROT_{rms})] \quad (9)$$

where the $3Dposerr_{norm}$ is the GDOP normalized 3D positioning errors, and the scintillation levels are represented by σ_φ , S4 and ROT_{rms} . It is clear from the above equations that the 3D positioning errors at high and low latitudes increase exponentially with increasing scintillation levels. This is in agreement with the results presented in Jacobsen and Dähn (2014), where they have shown that for high latitude receivers, located above 64°N, there is a strong positive correlation between 3D position errors and Rate of TEC index (ROTI), with the positioning errors increasing exponentially with increasing ROTI.

Sample results showing the validation of the models represented in (6) and (8) for days selected using the data sacrifice strategy described in the data and methodology section are shown, respectively, in Figs. 6 and 7. In the top panel of these figures, the black symbols indicate the observed values of the positioning errors, whereas the red lines indicate the model estimations. The bottom panels of Figs. 6 and 7 show the histogram of the residuals,

Table 4 Performance of the probability of loss of lock models as evaluated by the average R and average RMSE for the validation days at IQA station

Model	Validation days	Average R	Average RMSE	Number of validation days
$Prob\ lol_{scint}^{highlat}$	Scintillation	0.90	0.1930	39
$Prob\ lol_{scint}^{highlat}$	Non-Scintillation	0.82	0.1895	37
$Prob\ lol_{ROT}^{highlat}$	Scintillation	0.84	0.1885	39
$Prob\ lol_{ROT}^{highlat}$	Non-Scintillation	0.79	0.3227	37

Table 5 Performance of the probability of loss of lock models as evaluated by the average R and average RMSE for the validation days at BRO and NYA stations

Station	Model	Validation days	Average R	Average RMSE	Number of validation days
BRO	$Prob\ lo_{scint}^{highlat}$	Scintillation	0.86	0.1936	18
BRO	$Prob\ lo_{scint}^{highlat}$	Non-Scintillation	0.84	0.1716	18
BRO	$Prob\ lo_{ROT}^{highlat}$	Scintillation	0.77	0.2173	18
BRO	$Prob\ lo_{ROT}^{highlat}$	Non-Scintillation	0.70	0.2204	18
NYA	$Prob\ lo_{scint}^{highlat}$	Scintillation	0.88	0.1756	55
NYA	$Prob\ lo_{scint}^{highlat}$	Non-Scintillation	0.78	0.1802	55
NYA	$Prob\ lo_{ROT}^{highlat}$	Scintillation	0.75	0.1312	55
NYA	$Prob\ lo_{ROT}^{highlat}$	Non-Scintillation	0.73	0.2875	55

Table 6 Performance of the probability of loss of lock models as evaluated by the average R and average RMSE for the validation days at PRU station

Model	Validation days	Average R	Average RMSE	Number of validation days
$Prob\ lo_{scint}^{lowlat}$	Scintillation	0.84	0.0778	48
$Prob\ lo_{scint}^{lowlat}$	Non-Scintillation	0.74	0.2199	48
$Prob\ lo_{ROT}^{lowlat}$	Scintillation	0.73	0.2725	48
$Prob\ lo_{ROT}^{lowlat}$	Non-Scintillation	0.73	0.3500	48

Table 7 Performance of the probability of loss of lock models as evaluated by the average R and average RMSE for the validation days at POA and PAL stations

Station	Model	Validation days	Average R	Average RMSE	Number of validation days
POA	$Prob\ lo_{scint}^{lowlat}$	Scintillation	0.95	0.2159	12
POA	$Prob\ lo_{scint}^{lowlat}$	Non-Scintillation	0.88	0.1662	12
POA	$Prob\ lo_{ROT}^{lowlat}$	Scintillation	0.79	0.3491	12
POA	$Prob\ lo_{ROT}^{lowlat}$	Non-Scintillation	0.76	0.3395	12
PAL	$Prob\ lo_{scint}^{lowlat}$	Scintillation	0.91	0.1658	12
PAL	$Prob\ lo_{scint}^{lowlat}$	Non-Scintillation	0.88	0.2490	12
PAL	$Prob\ lo_{ROT}^{lowlat}$	Scintillation	0.76	0.3593	12
PAL	$Prob\ lo_{ROT}^{lowlat}$	Non-Scintillation	0.75	0.2330	12

defined as the difference between the observed and the model estimated positioning errors, along with the mean and the standard deviation.

It is worth noticing that the distribution of the residuals is well centered close to zero, with a mean = 0.0084 m in Fig. 6 and -0.0367 m in Fig. 7, i.e., the model estimation is accurate and that STD in Figs. 6 and 7, respectively, is 0.0285 m and 0.0364 m, providing the precision of the model estimations. The RMSE of the residuals in Figs. 6 and 7 is 0.0297 m and 0.0517 m, respectively. The low values for these statistical metrics indicate that the models were able to accurately estimate the values of the actual observed errors. The variations of the σ_ϕ and S4 scintillation indices are shown by blue lines in Figs. 6 and 7, respectively. More

importantly, it is possible to see, especially from Fig. 7 that the PPP solution has a convergence time of around 45 min, longer than expected, which is due to the effect of strong scintillation. It is to be noted that in the absence of scintillation, an accuracy at the level of a few cms is expected in the estimated 3D position components after the initial convergence period of about 20 min. Nevertheless, it can also be observed that during that period the model retrieves reasonably well the actual errors, confirming the ability of the model to estimate the effects of scintillation on the positioning solution properly. The results from the days selected using the data sacrifice strategy for the validation of the high and low latitude models represented in (6), (7), (8) and (9) are summarized in Tables 8 and 9, respectively.

Fig. 6 Top: Variations in the observed (black symbols), model estimated (red lines) 3D positioning errors and the phase scintillation index, σ_ϕ (blue lines); Bottom: Distribution of the residuals at BRO station on June 12, 2012

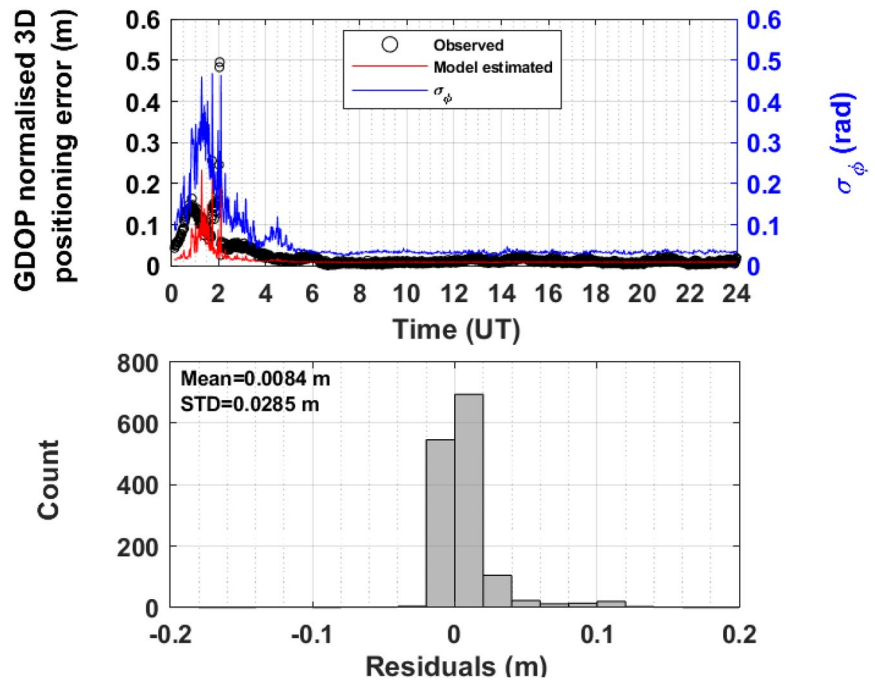
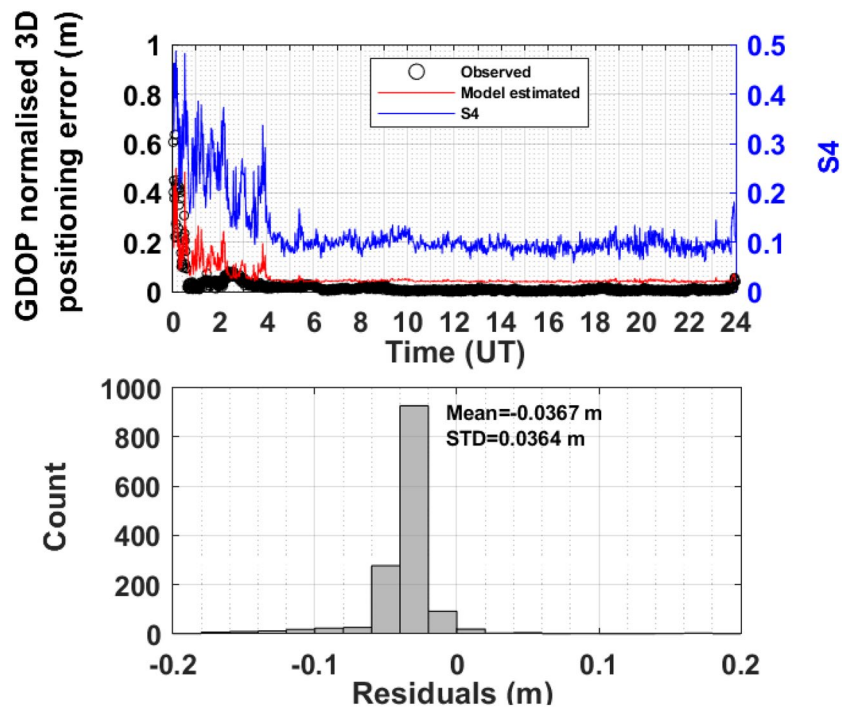


Fig. 7 Top: Variations in the observed (black symbols), the model estimated (red lines) 3D positioning errors and the amplitude scintillation index, S4 (blue lines); Bottom: Distribution of the residuals at PRU station on October 4, 2014



It can be observed from Tables 8 and 9 that the average RMSE values are all below 10 cm, which is within the expected positioning accuracy from an epoch-wise PPP solution (Bisnath and Gao 2009), thus suggesting a good performance of the developed models. Additionally, from Tables 8 and 9 it can be observed that the 3D positioning error models developed for the high and low latitudes as a function of ROT_{rms} i.e., (7) and (9), were validated using data recorded

at stations IQL and UFP, respectively. It was not possible to validate the performance of the developed models based on the scintillation indices, i.e., (6) and (8), as the stations IQL and UFP are, respectively, equipped with a Topcon NET-G3A and Trimble NETR9 receiver, which do not output the scintillation indices. On comparing the model performance during the scintillation and non-scintillation days at high and low latitudes, it can be observed from Tables 8 and 9

Table 8 Performance of the GDOP normalized 3D positioning error models as evaluated by the average RMSE for the validation days at high latitude stations IQA, BRO, NYA and IQL

Station	Model	Validation days	Average RMSE (m)	Number of validation days
IQA	$3D\ poserr_{norm}^{highlat\ scint}$	Scintillation	0.0321	39
IQA	$3D\ poserr_{norm}^{highlat\ scint}$	Non-Scintillation	0.0139	37
BRO	$3D\ poserr_{norm}^{highlat\ scint}$	Scintillation	0.0419	18
BRO	$3D\ poserr_{norm}^{highlat\ scint}$	Non-Scintillation	0.0274	18
NYA	$3D\ poserr_{norm}^{highlat\ scint}$	Scintillation	0.0169	55
NYA	$3D\ poserr_{norm}^{highlat\ scint}$	Non-Scintillation	0.0152	55
IQA	$3D\ poserr_{norm}^{highlat\ ROT}$	Scintillation	0.0332	39
IQA	$3D\ poserr_{norm}^{highlat\ ROT}$	Non-Scintillation	0.0132	37
BRO	$3D\ poserr_{norm}^{highlat\ ROT}$	Scintillation	0.0415	18
BRO	$3D\ poserr_{norm}^{highlat\ ROT}$	Non-Scintillation	0.0263	18
NYA	$3D\ poserr_{norm}^{highlat\ ROT}$	Scintillation	0.0171	55
NYA	$3D\ poserr_{norm}^{highlat\ ROT}$	Non-Scintillation	0.0167	55
IQL	$3D\ poserr_{norm}^{highlat\ ROT}$	Scintillation	0.0854	39
IQL	$3D\ poserr_{norm}^{highlat\ ROT}$	Non-Scintillation	0.0335	37

that although the average RMSE values at IQL and UFP stations are smaller than 10 cm, these are higher as compared to the other stations located in the same latitudinal sector. The average RMSE value during the scintillation days for the two high latitude stations IQL and IQA, located very close to each other, is 0.0854 m and 0.0332 m, respectively. Similarly, for the two closely located low latitude stations UFP and PRU the average RMSE values for the scintillation days are 0.0757 m and 0.0586 m, respectively. This suggests that the developed models presented here can provide a lower bound for positioning errors experienced by conventional receivers such as Trimble and Topcon.

Conclusion

The development and validation of statistical models to estimate the probability of loss of lock and GDOP normalized 3D positioning error developed under the EC funded IPS project have been presented. The statistical technique of nonlinear regression was applied to develop the models as a function of the scintillation levels represented by the phase and amplitude scintillation indices and the ROT_{rms} . Long-term data collected by ISMRs in operation at the

Table 9 Performance of the GDOP normalized 3D positioning error models as evaluated by the average RMSE for the validation days at low latitude stations PRU, POA, PAL and UFP

Station	Model	Validation days	Average RMSE (m)	Number of validation days
PRU	$3D\ poserr_{norm}^{lowlat\ scint}$	Scintillation	0.0525	48
PRU	$3D\ poserr_{norm}^{lowlat\ scint}$	Non-Scintillation	0.0375	48
POA	$3D\ poserr_{norm}^{lowlat\ scint}$	Scintillation	0.0391	12
POA	$3D\ poserr_{norm}^{lowlat\ scint}$	Non-Scintillation	0.0267	12
PAL	$3D\ poserr_{norm}^{lowlat\ scint}$	Scintillation	0.0469	12
PAL	$3D\ poserr_{norm}^{lowlat\ scint}$	Non-Scintillation	0.0283	12
PRU	$3D\ poserr_{norm}^{lowlat\ ROT}$	Scintillation	0.0586	48
PRU	$3D\ poserr_{norm}^{lowlat\ ROT}$	Non-Scintillation	0.0151	48
POA	$3D\ poserr_{norm}^{lowlat\ ROT}$	Scintillation	0.0228	12
POA	$3D\ poserr_{norm}^{lowlat\ ROT}$	Non-Scintillation	0.0136	12
PAL	$3D\ poserr_{norm}^{lowlat\ ROT}$	Scintillation	0.0189	12
PAL	$3D\ poserr_{norm}^{lowlat\ ROT}$	Non-Scintillation	0.0144	12
UFP	$3D\ poserr_{norm}^{lowlat\ ROT}$	Scintillation	0.0757	48
UFP	$3D\ poserr_{norm}^{lowlat\ ROT}$	Non-Scintillation	0.0670	48

high and low latitudes during the years of 2012–2015 was exploited to develop these models. The validation of the developed models was carried out at different stations covering a range of latitudes and equipped mostly with ISMRs, which yielded results that indicate their suitability to estimate the probability of satellite loss of lock and the 3D positioning errors over that range of latitudes. The validation results for the probability of loss of lock models at the high and low latitude stations indicated average R values above 0.7 and average RMSE values below 0.35, thus suggesting that the developed models perform well under scintillation and non-scintillation conditions. In the case of the 3D positioning error models, the validation results at the high and low latitudes indicated average RMSE values below 10 cm, suggesting a good performance of the models. Although the statistical model development and validation has been carried out using data from a limited number of ISMRs and conventional receivers, the encouraging results obtained indicate that these statistical models can be used to provide meaningful information to GNSS users under scintillation conditions.

Acknowledgment The research activities related to this paper at the Nottingham Geospatial Institute, University of Nottingham were funded by the EC funded IPS project [contract number: 434/PP/GRO/

RCH/15/8381]. This work was supported by the Engineering and Physical Sciences Research Council [Grant Number EP/H003479/1], data from BRO station are from a network of GNSS receivers established through the EPSRC research grant. Data from the PRU, POA and PAL stations in Brazil are part of the CIGALA/CALIBRA network. Monitoring stations from this network were deployed in the context of the Projects CIGALA and CALIBRA, both funded by the EC in the framework of the FP7-GALILEO-2009-GSA and FP7-GALILEO-2011-GSA-1a, respectively, and FAPESP Project Number 06/04008-2. Data from NYA station are from the network maintained by INGV. Authors thank Dr. Vincenzo Romano, Dr. Giorgiana De Franceschi, Dr. Lucilla Alfonsi and Dr. Ingrid Hunstad for the valuable support in maintaining the infrastructure and ensuring the quality of the NYA data.

Open Access This article is licensed under a Creative Commons Attribution 4.0 International License, which permits use, sharing, adaptation, distribution and reproduction in any medium or format, as long as you give appropriate credit to the original author(s) and the source, provide a link to the Creative Commons licence, and indicate if changes were made. The images or other third party material in this article are included in the article's Creative Commons licence, unless indicated otherwise in a credit line to the material. If material is not included in the article's Creative Commons licence and your intended use is not permitted by statutory regulation or exceeds the permitted use, you will need to obtain permission directly from the copyright holder. To view a copy of this licence, visit <http://creativecommons.org/licenses/by/4.0/>.

References

- Akala AO, Doherty PH, Carrano CS, Valladares CE, Groves KM (2012) Impacts of ionospheric scintillations on GPS receivers intended for equatorial aviation applications. *Radio Sci* 47(4):1–11. <https://doi.org/10.1029/2012RS004995>
- Aquino M, Sreeja V (2013) Correlation of scintillation occurrence with interplanetary magnetic field reversals and impact on global navigation satellite system receiver tracking performance. *Sp Weather* 11(5):219–224. <https://doi.org/10.1002/swe.20047>
- Basu S, Groves KM, Quinn JM, Doherty P (1999) A comparison of TEC fluctuations and scintillations at Ascension Island. *J Atmos Sol-Terr Phys* 61(16):1219–1226. [https://doi.org/10.1016/S1364-6826\(99\)00052-8](https://doi.org/10.1016/S1364-6826(99)00052-8)
- Basu S, Groves KM, Basu S, Sultan PJ (2002) Specification and forecasting of scintillations in communication/navigation links: current status and future plans. *J Atmos Sol-Terr Phys* 64(16):1745–1754. [https://doi.org/10.1016/S1364-6826\(02\)00124-4](https://doi.org/10.1016/S1364-6826(02)00124-4)
- Bisnath S, Gao Y (2009) Current state of precise point positioning and future prospects and limitations. In: Sideris M.G. (eds) *Observing our Changing Earth*. International Association of Geodesy Symposia 133: 615–623. https://doi.org/10.1007/978-3-540-85426-5_71
- Carrano CS, Groves KM (2010) Temporal decorrelation of GPS satellite signals due to multiple scattering from ionospheric irregularities. In: *Proceedings of ION GNSS 2010*, Institute of Navigation, Portland, OR, 361–374
- Doherty PH, Delay SH, Valladares CE, Klobuchar JA (2003) Ionospheric scintillation effects on GPS in the equatorial and Auroral regions. *J Inst Navig* 50(4):235–245. <https://doi.org/10.1002/j.2161-4296.2003.tb00332.x>
- Donahue B, Wentzel J, Berg R (2015) *Guidelines for RTK/RTN GNSS surveying in Canada*. Version 1.2. Natural Resources Canada: Geological Survey of Canada: Surveyor General Branch: Ontario Ministry of Transportation
- Humphreys TE, Psiaki ML, Ledvina BM, Kintner PM (2005) GPS carrier tracking loop performance in the presence of Ionospheric Scintillations. In: *Proceedings of ION GNSS 2005*, Institute of Navigation, Long Beach, CA, 156–167
- Jacobsen KS, Dähnn M (2014) Statistics of ionospheric disturbances and their correlation with GNSS positioning errors at high latitudes. *J Sp Weather Sp Clim* 4:A27. <https://doi.org/10.1051/swsc/2014024>
- Jayachandran PT et al (2009) The Canadian high arctic ionospheric network (CHAIN). *Radio Sci* 44(1):1. <https://doi.org/10.1029/2008RS004046>
- Jiao Y, Morton YT (2015) Comparison of the effect of high-latitude and equatorial ionospheric scintillation on GPS signals during the maximum of solar cycle 24. *Radio Sci* 50(9):886–903. <https://doi.org/10.1002/2015RS005719>
- Kintner PM, Kil H, Beach TL, de Paula ER (2001) Fading timescales associated with GPS signals and potential consequences. *Radio Sci* 36(4):731–743. <https://doi.org/10.1029/1999RS002310>
- Kintner PM, Ledvina BM, de Paula ER (2007) GPS and ionospheric scintillations. *Sp Weather* 5(9):S09003. <https://doi.org/10.1029/2006SW000260>
- Kouba J, P, Héroux (2001) Precise point positioning using IGS orbit and clock products. *GPS Solut* 5(2):12–28. <https://doi.org/10.1007/PL00012883>
- Malys S, Jensen PA (1990) Geodetic point positioning with GPS carrier beat phase data from the CASA UNO experiment. *Geophys Res Lett* 17(5):651–654. <https://doi.org/10.1029/GL017i005p00651>
- Pi X, Mannucci AJ, Lindqwister UJ, Ho CM (1997) Monitoring of global ionospheric irregularities using the worldwide GPS network. *Geophys Res Lett* 24(18):2283–2286. <https://doi.org/10.1029/97GL02273>
- Pi X, Mannucci AJ, Valant-Spaight B, Bar-Sever Y, Romans LJ, Skone S, Sparks L, Hall GM (2013) Observations of Global and Regional Ionospheric Irregularities and Scintillation Using GNSS Tracking Networks. In: *Proceedings of the ION Pacific PNT Meeting 2013*, Honolulu, Hawaii, 752–761
- Pi X, Lijima BA, Lu W (2017) Effects of ionospheric scintillation on GNSS. *J Inst Navig* 64(1):3–22. <https://doi.org/10.1002/navi.182>
- Rodrigues FS, Aquino M, Dodson A, Moore T, Waugh S (2004) Statistical analysis of GPS ionospheric scintillation and short-time TEC variations over Northern Europe. *J Inst Navig* 51(1):59–75. <https://doi.org/10.1002/j.2161-4296.2004.tb00341.x>
- Seber GAF, Wild CJ (2003) *Nonlinear regression*. Wiley-Interscience, Hoboken, NJ
- Septentrio PolaRxS (2010) *Septentrio PolaRxS application manual version 1.0.0*
- Skone S, Kundsén K, de Jong M (2001) Limitations in GPS receiver tracking performance under ionospheric scintillation conditions. *Phys Chem Earth (A)* 26(6–8):613–621. [https://doi.org/10.1016/S1464-1895\(01\)00110-7](https://doi.org/10.1016/S1464-1895(01)00110-7)
- Spogli L, Alfonsi L, De Franceschi G, Romano V, Aquino M, Dodson A (2009) Climatology of GPS ionospheric scintillations over high and mid-latitude European regions. *Ann Geophys* 27(9):3429–3437. <https://doi.org/10.5194/angeo-27-3429-2009>
- Sreeja V et al (2011) Tackling ionospheric scintillation threat to GNSS in Latin America. *J Sp Weather Sp Clim* 1(1):A05. <https://doi.org/10.1051/swsc/2011005>
- Sreeja V, Aquino M, Elmas ZG, Forte B (2012) Correlation analysis between ionospheric scintillation levels and receiver tracking performance. *Sp Weather* 10(6):S06005. <https://doi.org/10.1029/2012SW000769>
- Vadakke Veetil S, Aquino M, Spogli L, Cesaroni C (2018) A statistical approach to estimate Global Navigation Satellite Systems (GNSS) receiver signal tracking performance in the presence of

ionospheric scintillation. *J Sp Weather Sp Clim* 8:A51. <https://doi.org/10.1051/swsc/2018037>

- Veetttil SV, Aquino M, De Franceschi G, Spogli L, Cesaroni C, Romano V (2018b) Statistical models to provide meaningful information to GNSS end-users under ionospheric scintillation conditions. In: Proceedings of ION GNSS 2018, Institute of Navigation, Miami, Florida, 3827–3832. doi: <https://doi.org/https://doi.org/10.33012/2018.16034>
- Vadakke Veetttil S et al (2019) The ionosphere prediction service prototype for GNSS users. *J Sp Weather Sp Clim* 9:A41. <https://doi.org/10.1051/swsc/2019038>
- Van Dierendonck AJ, Klobuchar J, Hua Q (1993) Ionospheric scintillation monitoring using commercial single frequency C/A code receivers. In: Proceedings of ION GPS 1993, Institute of Navigation, Salt Lake City, UT, 1333–1342
- Yang Z, Liu Z (2017) Investigating the inconsistency of ionospheric ROTI indices derived from GPS modernized L2C and legacy L2 P(Y) signals at low-latitude regions. *GPS Solut* 21(2):783–796. <https://doi.org/10.1007/s10291-016-0568-3>
- Zumberge JF, Heflin MB, Jefferson DC, Watkins MM, Webb FH (1997) Precise point positioning for the efficient and robust analysis of GPS data from large networks. *J Geophys Res Solid Earth* 102(B3):5005–5017. <https://doi.org/10.1029/96JB03860>

Publisher's Note Springer Nature remains neutral with regard to jurisdictional claims in published maps and institutional affiliations.



S. Vadakke Veetttil is a senior research fellow at the Nottingham Geospatial Institute of the University of Nottingham in the UK, involved in the European Commission, European Space Agency and UK research council funded projects. Her research focuses on assessing the effects of space weather on GNSS receivers and positioning errors aiming to improve the modeling of scintillation and to develop scintillation mitigation tools.



M. Aquino is a retired Associate Professor at the Nottingham Geospatial Institute of the University of Nottingham in the UK. He pioneered the deployment of ionospheric scintillation and TEC monitoring receivers in Northern Europe in 2001. His research has focused on ionospheric effects on GNSS, including system vulnerability to ionospheric disturbances and relevant countermeasures.